Title

Numerical simulations of larval transport into a rip-channeled surf zone

Journal

Limnology and Oceanography, 59(4)

ISSN

0024-3590

Authors

Fujimura, Atsushi G
Reniers, Ad JHM
Paris, Claire B
et al.

Publication Date

2014-07-01

DOI

10.4319/lo.2014.59.4.1434

Peer reviewed

Limnol. Oceanogr., 59(4), 2014, 1434–1447

doi:10.4319/lo.2014.59.4.1434

Numerical simulations of larval transport into a rip-channeled surf zone

Atsushi G. Fujimura,[1,*] Ad J. H. M. Reniers,[1] Claire B. Paris,[1] Alan L. Shanks,[2] Jamie H. MacMahan,[3] and Steven G. Morgan [4]

[1] Rosenstiel School of Marine and Atmospheric Science, University of Miami, Miami, Florida
[2] Oregon Institute of Marine Biology, University of Oregon, Charleston, Oregon
[3] Department of Oceanography, Naval Postgraduate School, Monterey, California
[4] Bodega Marine Laboratory, University of California Davis, Bodega Bay, California

Abstract

Competent larvae of intertidal invertebrates have to migrate toward shore for settlement; however, their migration through the surf zone is not understood. We investigated larval transport mechanisms at a rip-channeled beach. Because tracking larvae in the surf zone is infeasible, we used a three-dimensional biophysical model to simulate the processes. The coupled model consists of a physical module for currents and waves, and a biological module for adding larval traits and behaviors as well as Stokes drift to Lagrangian particles. Model calculations were performed with and without onshore wind forcing. Without wind, wave-driven onshore streaming occurs in the bottom boundary layer outside the surf zone. With onshore wind, onshore currents occur near the surface. In the surf zone, offshore-directed rip currents and compensating onshore-directed currents over shoals are formed in both no-wind and wind cases. In the biological module, neutral, negative, and positive buoyant particles were released offshore. Additionally, particles either sank in the presence of turbulence or not. Two scenarios achieved successful onshore migration: Negatively buoyant larvae without wind forcing sink in the turbulent bottom boundary layer and are carried onshore by streaming; positively buoyant larvae drift toward shore in wind-driven surface currents to the surf zone, then sink in the turbulent surf zone and remain near the bottom while transported shoreward. In both cases, the larval concentration is highest in the rip channel, consistent with field data. This successful result is only obtained if turbulence-dependent sinking behavior and Stokes drift are included in the transport of larvae.

Larval recruitment is an important element in the dynamics and structure of marine populations and communities. Larvae of many intertidal invertebrates cross the surf zone, develop in the open ocean, and migrate back to the shore at the end of the larval stage (Morgan et al. 2009*c*; Shanks and Shearman 2009). Most invertebrate larvae are slow swimmers that regulate depth and likely depend on currents and other physical forcing to transport them onshore for settlement (Queiroga and Blanton 2005). In upwelling regimes along the western margins of continents, a widely accepted hypothesis is that larvae of intertidal invertebrates are swept offshore during wind-driven upwelling events (Connolly et al. 2001). However, recent studies conducted in northern California (Morgan et al. 2009*b*, *c*; Morgan and Fisher 2010) and southern Oregon (Shanks and Shearman 2009) revealed that the onshore transport of larvae of many invertebrates is not limited by upwelling. Additionally, larvae of most species were not carried far offshore by upwelling nor onshore by downwelling, but were found at all times within several kilometers of shore; competent larvae were abundant within a kilometer from shore during the summer (Shanks and Shearman 2009; Morgan and Fisher 2010). More importantly, onshore recruitment of these competent larvae was spatially and temporally variable, suggesting the hypothesis that the surf zone may represent a semipermeable barrier to cross-shore exchange (Rilov et al. 2008; Shanks et al. 2010). Local processes within the surf zone are important for the migration of the larvae of intertidal invertebrate; however, the mechanism of larval delivery across this barrier is not understood.

There are a number of possible physical transport mechanisms that need to be considered. At a heterogeneous shore with alongshore-sandbars, shoals and rip channels produce rip currents, which can enhance cross-shore exchange (MacMahan et al. 2010). Onshore transport mainly occurs over shoals where wave breaking occurs, driving onshore flows that diverge toward the shore and subsequently feed strong offshore-directed rip currents. Rip-channeled beaches are common and observed around the world. This rip-channeled system of alongshore variability-induced exchange is generally found at intermediate (gradual beach slope) beaches and not at reflective (steep beach slope) beaches (Wright and Short 1984), which is consistent with observations by Shanks et al. (2010), who showed that recruitment was higher on mildly sloping beaches than on steep beaches.

Stokes drift (Stokes 1847) is a time-averaged volume transport current in the direction of wave propagation, and it may slowly transport larvae toward shore. This mechanism may be active at dissipative beaches, but might not or only partially be supported at reflective beaches because Stokes drift is associated with progressive surface gravity waves only, and steep beaches reflect waves with a wide range of frequencies resulting in (partially) standing waves. Stokes drift is explained further in the Methods section.

* Corresponding author: afujimura@rsmas.miami.edu

Cross-shore wind forcing also can increase cross-shore exchange (Fewings et al. 2008). Surface mass transport is in the direction of wind forcing, so onshore wind may push larvae near the surface toward shore. For offshore wind or weak wind conditions, surface currents flow in the opposite direction (Lentz et al. 2008).

Wave stress in the bottom boundary layer generates persistent streaming in the direction of wave propagation (Longuet-Higgins 1953). Although streaming velocities are small (O, cm s^{-1}), over time, they may cause onshore transport of larvae near the bottom.

In addition to the physical forcing, biological factors such as buoyancy, sinking rate, and depth preferences of larvae may be important. By regulating their depth, larvae of some species recruit onshore in surface waters, whereas other species recruit onshore near the bottom in upwelling regimes (Morgan et al. 2009*a*). Furthermore, larvae of various invertebrate taxa sink under turbulent conditions (Fuchs et al. 2004, 2013; Roy et al. 2012). We hypothesize that depth preferences and sinking behavior help larvae to avoid strong offshore currents or enter the surf zone in streaming currents.

Tracking larvae in a very turbulent and rough environment is not feasible. However, biophysical numerical modeling allows examining the discrete and combined roles of physical and biological processes in the surf zone. Particularly, an Individual Based Model (IBM) with complex hydrodynamics is quite useful for modeling microscopic organisms in various flow conditions and has been extensively used in population connectivity studies (Paris et al. 2007). Based on a similar technique, we test possible mechanisms of onshore larval delivery by using a newly established coupled modeling system (Paris et al. 2013*b*). In this study, we aim at identifying potential mechanisms of onshore larval transport, focusing on the effects of Stokes drift, wind forcing, and vertical motions of larvae (i.e., buoyancy and sinking behavior). We also test the effects of random wave groups that could generate more realistic situations, such as infragravity waves and surf zone eddies, than regular waves (MacMahan et al. 2004; Reniers et al. 2010).

Methods

Field work—We collected physical data and biological samples at Sand City beach, Monterey Bay, California in the summer of 2010 (Fig. 1A). The location is characterized as an intermediate beach (moderate beach slope; Wright and Short 1984) with well-formed rip channels and shoals. Bathymetric data used for the model grid were collected with a personal watercraft equipped with sonar and a Global Positioning System (GPS), and for the near shore, a person walking with a GPS. The alongshore-average beach profile consists of 1/7.5 intertidal beach slope, 1/57 surf zone slope, and 1/25 offshore profile. Alongshore variability in the beach profile is apparent in Fig. 1B. Current and wave data were obtained by acoustic Doppler current profilers located at 11 m water depth.

Replicate plankton samples were collected repeatedly for 30 d (15 June to 15 July 2010) at three locations: offshore just outside the surf zone (inner shelf), rip channel, and shoal (Fig. 1B). Within the rip channel and on the shoal, a zooplankton net with 202 μm mesh and a 25 cm diameter equipped with a flow meter was used to collect the samples as the horizontal flow pushed through the net. Just outside of the surf zone, an identical net was used to collect the zooplankton samples by hauling the net from the bottom to the surface. A summary graph of zooplankton concentrations at the three locations is shown in the discussion section to compare with the model output.

Hydrodynamic model—The numerical simulation software package Delft3D was used to perform three-dimensional hydrodynamic model simulations of the nearshore. The Delft3D hydrodynamic model comprises FLOW (Deltares 2013*a*) and WAVE (Deltares 2013*b*) modules.

The model domain formed of 850 m in the alongshore direction, 450 m in cross-shore direction, and collected bathymetry data determined depths. A regular grid (hexahedral cells) was used for the model mesh. Spacing of grid cells was 10 m alongshore, $\sim$ 5–10 m cross-shore with the finest resolution at the shoreline, and 14 σ-layers were applied for vertical spacing, which become finer toward the bottom to resolve boundary-layer streaming. Shoreline reflections were managed by an offshore Riemann boundary, a weakly reflective open boundary, while the other sides (onshore and alongshore) were closed. Turbulence was modeled with a k–ε closure scheme (Deltares 2013*a*), with transport equations to solve turbulent kinetic energy (k) and energy dissipation rate (ε).

Shore normal waves, based on the average wave data during the biological sampling period (significant wave height = 0.75 m, peak wave period = 8.75 s), were generated at the offshore boundary. We applied two wave conditions: regular normally incident waves and random wave groups by using the Joint North Sea Wave Project spectrum (Hasselmann et al. 1973). We also tested effects of wind surface stress by applying either no wind (0 m s^{-1}) or constant onshore wind (8.0 m s^{-1}), which represent minimal and peak wind speeds measured during the field experiment, respectively.

Run time was 2 h with a time step of 3 s, and intervals of output and communication between FLOW and WAVE were 6 s. Because no diurnal events (tide, various wind, etc.) were considered, the 2 h simulation output was used periodically for a 24 h larval-transport simulation. The model domain and bathymetry are shown in Fig. 1B.

Larval transport model—Modeled physical parameters, such as currents, waves, bathymetry, eddy diffusivities, and turbulence, were transferred to a biological module. This module was adapted from the Connectivity Modeling System (CMS, Paris et al. 2013*b*), which is a coupled multi-scale biophysical IBM, based on a stochastic Lagrangian framework. The CMS code was rewritten in a MATLAB with some modifications to directly import the physical model output. The imported outputs include the bathymetry, water levels, flow velocities, wave information, eddy diffusivities, and turbulent-energy dissipation rate every 6 s.

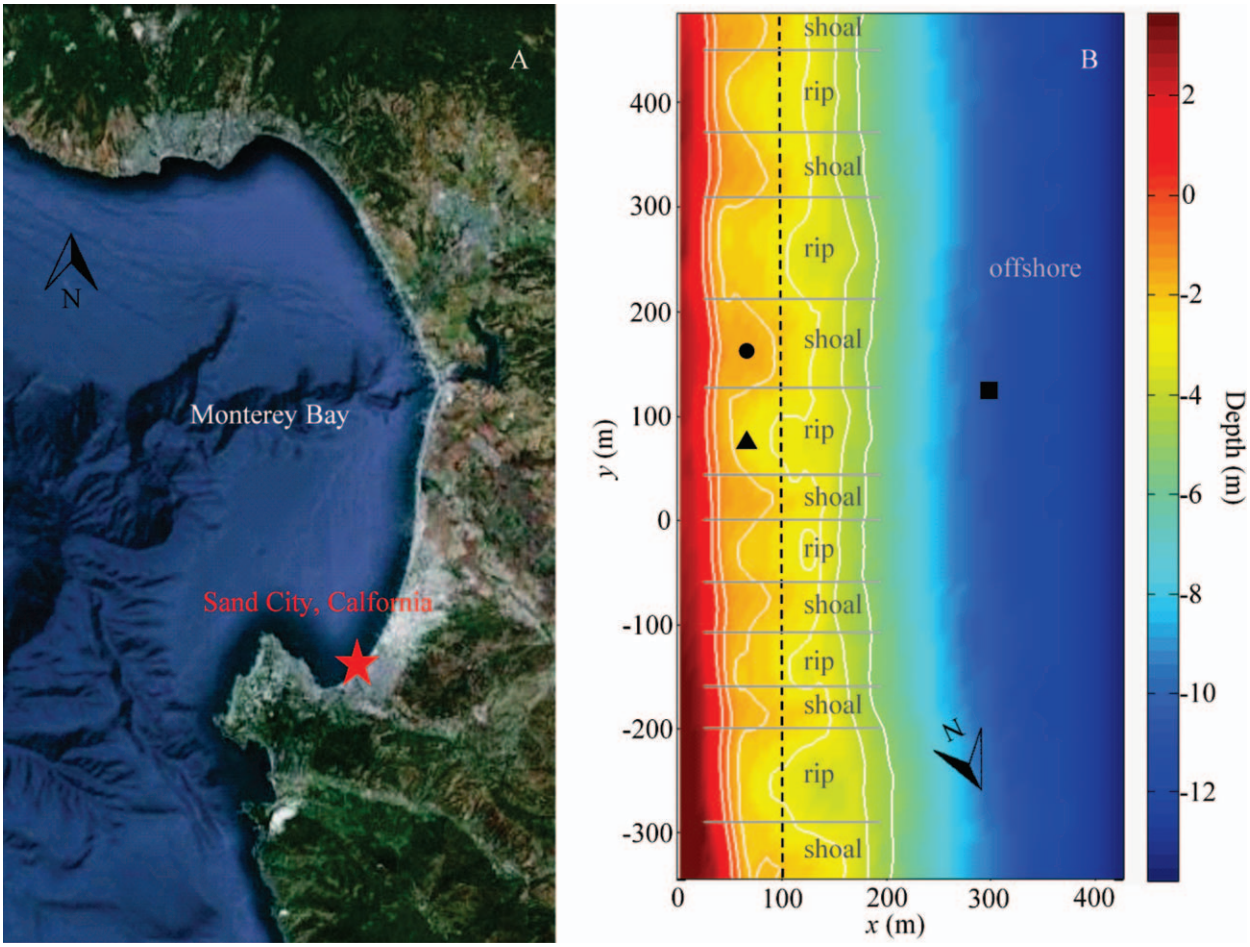

Fig. 1. (A) The study site is indicated by a red star (credit: Google Earth). (B) Bathymetry in the model domain. White isobaths are in 1 m increments from 0 m (shoreline) to 5 m. The approximate edge of the surf zone is shown as a black dashed line. North is to the bottom. Rip channel and shoal ranges are shown. The approximate plankton sampling locations are indicated in a circle for the shoal, a triangle for the rip channel, and a square for offshore.

A fourth-order Runge–Kutta method was used for integration of the advection part, both in time and space following Paris et al. (2013*b*):

$$k_1 = f\left(\vec{U}_i, t_i\right)\Delta t \tag{1}$$

$$k_2 = f\left(\vec{U}_i + \frac{k_1}{2}, t_i + \frac{\Delta t}{2}\right)\Delta t \tag{2}$$

$$k_3 = f\left(\vec{U}_i + \frac{k_2}{2}, t_i + \frac{\Delta t}{2}\right)\Delta t \tag{3}$$

$$k_4 = f\left(\vec{U}_i + k_3, t_i + \Delta t\right)\Delta t \tag{4}$$

$$\vec{U}_{i+1} = \vec{U}_i + \frac{k_1 + 2k_2 + 2k_3 + k_4}{6} \tag{5}$$

where $\vec{U}$ is the velocity of water current at ith time step. The integration time step size Δt was 6 s, where the spatial resolution is the same as the one used in the physical model.

The velocity $\vec{U}$ in Eqs. 1–5 was set as either Eulerian (background) velocity or Lagrangian (particle tracking) velocity to test the effect of Stokes drift. Their relationship is,

$$\vec{U}_L = \vec{U}_E + \vec{U}_S \tag{6}$$

where $\vec{U}_L$ is the Lagrangian velocity, $\vec{U}_E$ is the Eulerian velocity, and $\vec{U}_S$ is Stokes drift written as,

$$\vec{U}_S = \frac{\omega k a^2 \cosh(2k(H+z))}{2\sinh^2(kH)}(\cos\phi, \sin\phi) \tag{7}$$

where ω is the radial wave frequency, k is the radial wave number, a is the wave amplitude, H is the local water depth, z is the vertical position of a particle with $z = 0$ at mean sea level, and ϕ is the wave angle. In this paper, we neglected potential entrainment of particles in the breaking wave roller (Feddersen 2007; Reniers et al. 2013), which may contribute to the preferential transport of surface material from the shoals to the rip channels that experience less

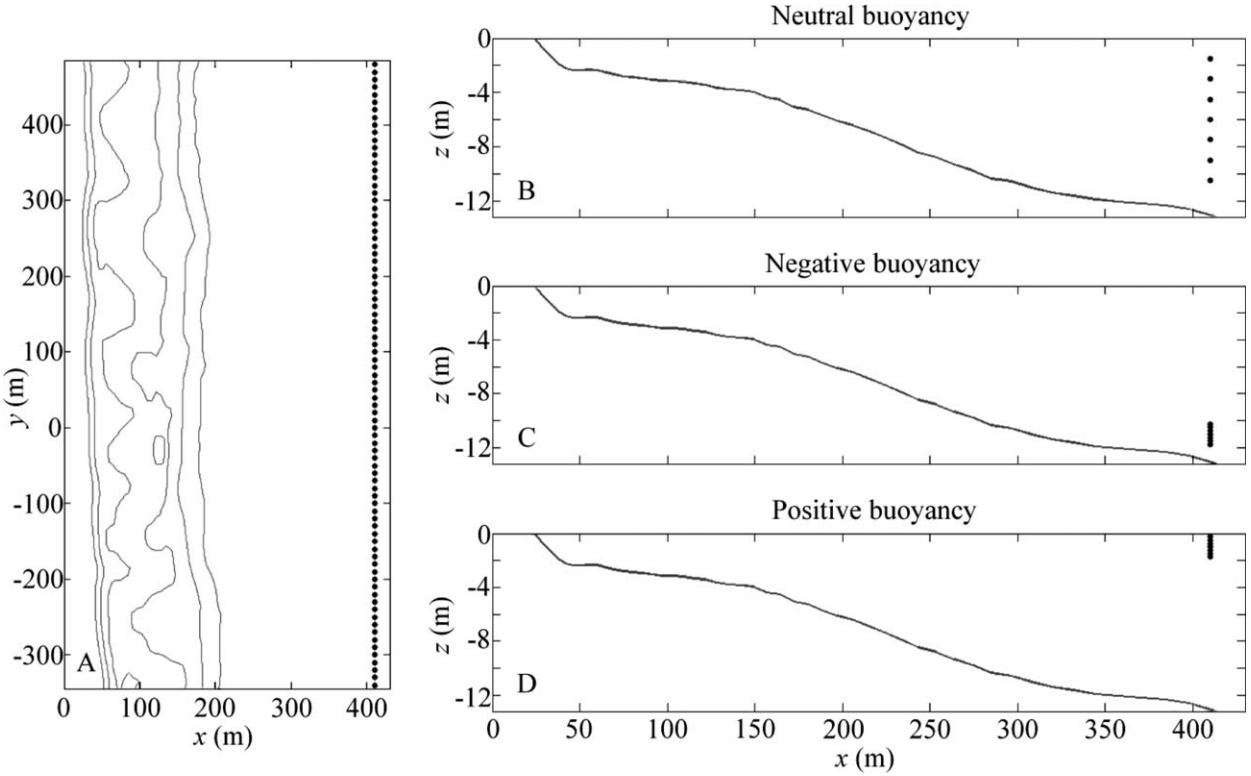

Fig. 2. Initial location of particles shown in black dots. (A) Horizontal distribution for all types of particles. Bottom contour lines from 0 m depth (shore line) to 5 m depth with 1 m increments are given. Vertical distributions of (B) neutrally buoyant, (C) negatively buoyant, and (D) positively buoyant particles. The maximum depth line is shown in gray.

wave breaking due to their increased depth, but at present cannot be resolved within our three-dimensional modeling approach.

We applied a random walk to each particle to account for subgrid-scale turbulence. This was modeled by adding random velocities u_{diff}, v_{diff}, w_{diff} of all three spatial components (cross-shore, alongshore, and vertical direction, respectively) calculated by,

$$u_{\text{diff}} = n\sqrt{\frac{2K_h}{\Delta t}} \tag{8}$$

$$v_{\text{diff}} = n\sqrt{\frac{2K_h}{\Delta t}} \tag{9}$$

$$w_{\text{diff}} = n\sqrt{\frac{2K_v}{\Delta t}} \tag{10}$$

where n is a Gaussian random number, K_h and K_v are horizontal and vertical eddy diffusivities, respectively.

Each particle was assigned a vertical velocity w_b, which represents buoyancy or vertical swimming speed of the larva. We tested three types of w_b: 0 m s^{-1} (neutrally buoyant), -10^{-3} m s^{-1} (negatively buoyant) and 4×10^{-3} m s^{-1} (positively buoyant) based on Fuchs et al. (2004). No active horizontal swimming behavior was considered here.

We also tested a scenario that a larva stops swimming vertically and sinks by its own weight in the presence of turbulence. According to Fuchs et al. (2004), competent larvae sink at $w_s = -10^{-2}$ m s^{-1} when the turbulent energy dissipation rate is $\varepsilon > 10^{-5}$ m^2 s^{-3}. In this paper, this type of behavior is called sinking behavior.

Thus, the total velocity components u_{tot} (cross-shore), v_{tot} (alongshore), and w_{tot} (vertical) are,

$$u_{\text{tot}} = u_{\text{adv}} + u_{\text{diff}} \tag{11}$$

$$v_{\text{tot}} = v_{\text{adv}} + v_{\text{diff}} \tag{12}$$

$$w_{\text{tot}} = \begin{cases} w_{\text{adv}} + w_{\text{diff}} + w_b & \text{if the sinking behavior is off} \\ w_{\text{adv}} + w_{\text{diff}} + w_b & \varepsilon < 10^{-5}\text{m}^2\text{s}^{-3} \\ w_{\text{adv}} + w_{\text{diff}} + w_s & \varepsilon \geq 10^{-5}\text{m}^2\text{s}^{-3} \end{cases} \tag{13}$$

where u_{adv}, v_{adv}, and w_{adv} are advection flow velocities of the three spatial components from Eq. 5. And then, a new position of the particle is,

$$\vec{X}_{i+1} = \vec{X}_i + \vec{U}_{\text{tot}}\Delta t \tag{14}$$

where $\vec{X}_i$ is the old position of all three spatial components and $\vec{U}_{\text{tot}}$ is the total velocity obtained from Eqs. 11–13.

During a 24 h simulation, 602 particles (86 × 7 array) were released every hour from offshore ($x = 410$ m) equally distributed alongshore ($\Delta y = 10$ m) at three vertical locations for each type of particle: near the bottom for the particles with negative buoyancy, near the water surface for the ones with positive buoyancy, and dispersed through water column for the ones with neutral buoyancy (Fig. 2).

Table 1. Performed model cases. In the 'Wave' column, 'regular' is regular incident wave, and 'group' is random wave group. 'Wind' is either no wind (0 m s^{-1}) or onshore wind (8.0 m s^{-1}). w_s = sinking behavior of particles, included (on) or not (off). w_b = vertical velocity of particles. $\vec{U}_S$ = Stokes drift, either included (on) or not (off). Each case name describes a test condition: 's' if sinking behavior is included; 'w' if onshore wind is included; '0', '−', or '+' correspond to neutral, negative, or positive buoyancy of particles, respectively.

Case	Wave	Wind (m s^{-1})	w_s	w_b (m s^{-1})	$\vec{U}_S$
1.0	regular	0	off	0	on
2.−	regular	0	off	-10^{-3}	on
3.+	regular	0	off	4×10^{-3}	on
4.s0	regular	0	on	0	on
5.s−	regular	0	on	-10^{-3}	on
6.s+	regular	0	on	4×10^{-3}	on
7.w0	regular	8.0	off	0	on
8.w−	regular	8.0	off	-10^{-3}	on
9.w+	regular	8.0	off	4×10^{-3}	on
10.ws0	regular	8.0	on	0	on
11.ws−	regular	8.0	on	-10^{-3}	on
12.ws+	regular	8.0	on	4×10^{-3}	on
13.s−	regular	0	on	-10^{-3}	off
14.ws+	regular	8.0	on	4×10^{-3}	off
15.s−	group	0	on	-10^{-3}	on
16.ws+	group	8.0	on	4×10^{-3}	on

The number of particles and the release frequency are due to limited computational ability, but sufficient for the main purpose because our sensitivity analysis, as recommended by North et al. (2009), showed that the main results did not change with at least half the number of particles. Offshore and alongshore boundaries were set as outlets, so once a particle crossed one of the boundaries, it was no longer taken into account. The first 12 h run was used as a spin-up stage for particle initialization. The second half of the simulation (12–24 h) was used to calculate the time-averaged number of particles. The test cases and model parameters are summarized in Table 1.

Results

For case notation: '0', '−', and '+' corresponds to neutral, negative, and positive buoyancy of particles, respectively; 's' means sinking behavior is included; and 'w' is onshore wind is included (Table 1).

No-wind case—Particles in Cases 1.0, 3.+, and 6.s+ did not reach the surf zone (Fig. 3). Particles in Cases 2.− and 4.s0 partially entered the surf zone, while particles in Case 5.s− were dominant within the surf zone (Fig. 3). The negatively buoyant particles with sinking behavior stayed closer to the bottom than ones without the sinking behavior (Fig. 4A). Relatively large numbers of particles stayed on offshore bottom longer (Fig. 4A) because the particle releasing location was there and bed current (streaming) offshore was weaker than close-shore (Fig. 4B).

In the no-wind case, vertical profiles of cross-shore velocity consistently showed onshore currents near the bed at x = 125 m and farther offshore (Fig. 4B). Note that the rip and shoal velocities in Fig. 4B are alongshore- and time-averaged velocities of all defined rip channels and shoals. The averaging masks episodic strong rip-current velocities (Reniers et al. 2010). Within the surf zone (at x = 75 and 100 m), the Eulerian velocities showed offshore currents; however, by adding Stokes drift (= Lagrangian velocity), bottom flow changed to onshore, while the surface current was still offshore, except on the shoal at x = 75 m where Lagrangian velocities were onshore throughout the water column.

Onshore-wind case—Particles in Cases 7.w0, 8.w−, and 11.ws− did not reach the surf zone (Fig. 5). Particles in Cases 9.w+ and 10.ws0 partially crossed the surf zone, while those in Case 12.ws+ were dominant in the surf zone (Fig. 5). The positively buoyant particles were near the surface in Case 9.w+ and outside of the surf zone in Case 12.ws+. The particles with sinking behavior sank in the surf zone (Fig. 6A).

Wind forcing altered the cross-shore velocity vertical profiles (Fig. 6B). Again, these velocities are alongshore- and time-averaged velocities. Streaming was suppressed and surface water flowed toward shore at x = 200, 300, and 400 m. Similar to the no-wind case, at x = 75, 100, and 125 m the Eulerian velocity showed an offshore current; however, the Lagrangian velocity near the bed changed to an onshore current, while the surface current still flowed offshore in the rip at x = 75 and 100 m and on the shoal at x = 125 m. Lagrangian velocities in the entire water column at x = 75 m were onshore.

Cases with high onshore migration rate—Cases 5.s− (regular waves, no wind, Stokes drift, negative buoyant particles with the sinking behavior) and 12.ws+ (regular waves, wind, Stokes drift, positive buoyant particles with the sinking behavior) are two scenarios in which particles successfully migrated to the shore by crossing the surf zone. Seventeen percent and 12% of entire particles exited from the alongshore outlets in Cases 5.s− and 12.ws+, respectively, so these cases in Figs. 3 and 5 represent most particles. The following subsections show other characteristics of these cases, and corresponding cases with different physical parameters.

Effects of Stokes drift and wave group—When Stokes drift was not included, most particles that were able to cross the surf-zone barrier in Cases 5.s− and 12.ws+ were not able to enter the surf zone in Cases 13.s− and 14.ws+, respectively (Fig. 7A).

Random-wave group forcing altered the patterns of particle distributions (Fig. 7B). Particles in Case 5.s− and 12.ws+ were approximately evenly distributed in rip channels; however, those with wave groups (i.e., Cases 15.s− and 16.ws+, respectively) were patchier. Rip ejections can be seen at the head of rip channels (x = 200 ± 30 m) in Case 16.ws+.

Discussion

Our model study shows both physical forcing (i.e., waves and currents) and biological processes (i.e., vertical position

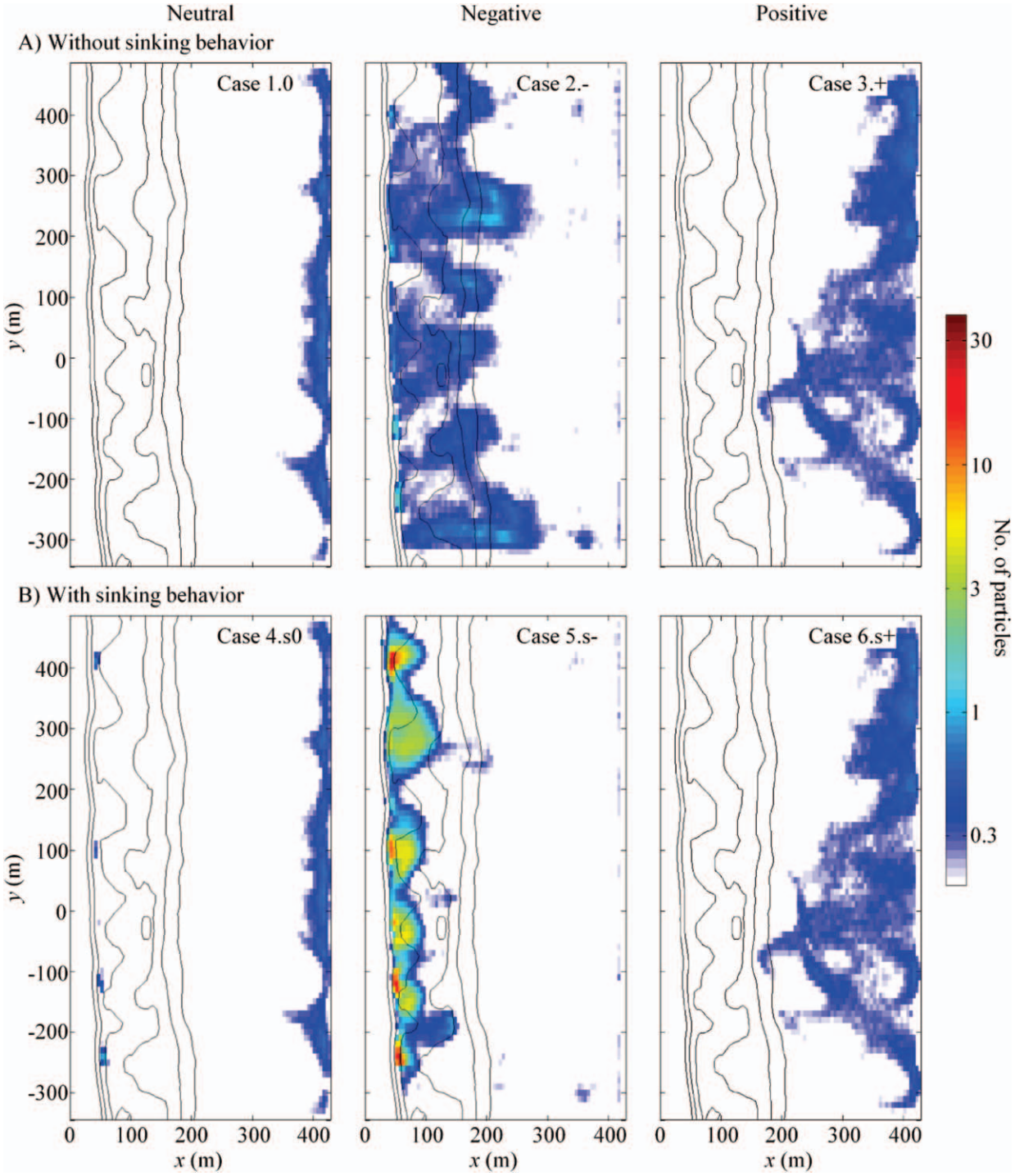

Fig. 3. Depth- and time-averaged number of particles per grid cell. Regular wave, no wind, Stokes drift, with buoyancy of neutral (Cases 1.0 and 4.s0), negative (Cases 2.− and 5.s−), and positive (Cases 3.+ and 6.s+). (A) Particles without sinking behavior, and (B) particles with sinking behavior. Bottom contour lines from 0 m depth (shore line) to 5 m depth with 1 m increments are given. The color bar is in a log scale.

within the water column and sinking in turbulence) may play important roles in the onshore migration of larvae. Although it is theoretical, the model results give us an idea of how larval behavior, which is hard to demonstrate and observe in the field, may affect the entrance of larvae into the surf zone.

To enter the surf zone from offshore, larvae need to have the sinking behavior described by Fuchs et al. (2004). Recent studies revealed turbulence-induced downward movement can be seen in other intertidal invertebrates (Roy et al. 2012; Fuchs et al. 2013), so this behavior seems to be common in many intertidal larvae. In addition to

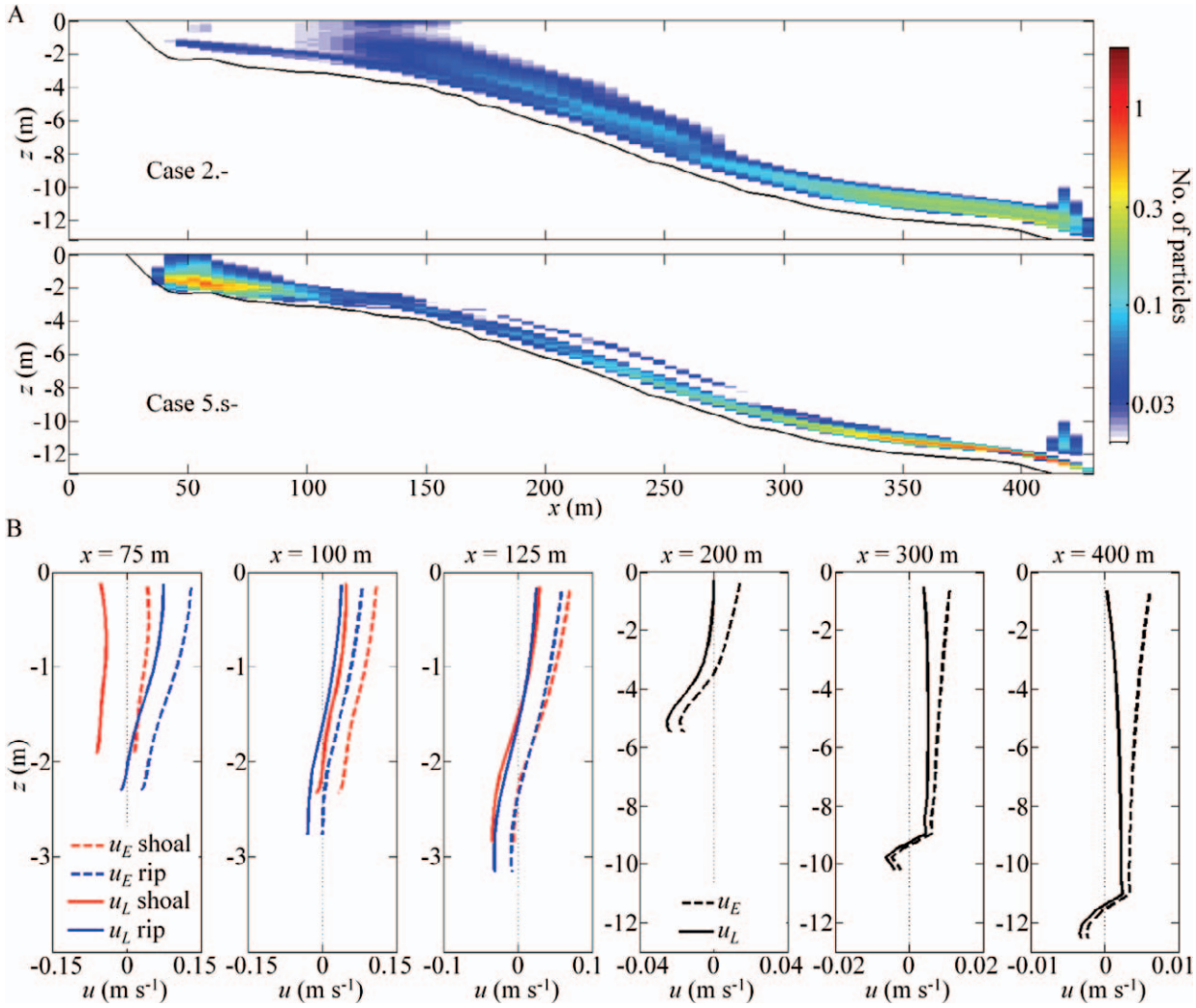

Fig. 4. (A) Alongshore- and time-averaged number of particles per grid cell. Regular wave, no wind, Stokes drift, negative buoyancy, without sinking behavior (Case 2.−) and with sinking behavior (Case 5.s−). The maximum depth line is shown as a bottom frame. The color bar is in a log scale. (B) Vertical profiles of alongshore- and time-averaged cross-shore velocities in the physical model case of regular waves without wind. Dashed line is Eulerian velocity (u_E) and solid line is Lagrangian velocity (u_L). The first three panels to the left are average velocities in the rip channels (blue) and on the shoals (red), and the others are averages over the total alongshore ranges (black). Positive values correspond to offshore currents.

vertical movement, horizontal swimming (which we ignored because we focused on the importance of vertical motions of weak swimmers) could also help for the cross-shore migration by relatively strong swimmers such as fish and crab larvae. Staaterman et al. (2012) showed the significance of horizontal swimming for larval settlement by using a similar biophysical model scheme. The horizontal swimming direction might be determined by sound (Vermeij et al. 2010), sunlight (Shanks 1995), chemical signals (Paris et al. 2013*a*), and other environmental stimuli (reviewed by Kingsford et al. 2002). These orientation behaviors should be the subject of future studies to better understand how strongly swimming larvae may cross the surf zone.

Stokes drift appears to be essential for larvae to enter the surf zone, and our results are consistent with the computational drifter results reported by Reniers et al. (2009). By including Stokes drift, the cross-shore velocities near the bed at the approximate edge of the surf zone (x = 100 m) and at x = 125 m both with and without wind, as well as in rip channels at x = 75 m in no-wind case (where the most larvae sink because of the high turbulence), were changed from offshore-directed to onshore (Figs. 4B, 6B). Cross-shore transport rates change with wave conditions because it affects Stokes drift, wave breaking, and surf zone eddies as well as the general rip-current circulation and as such will be important in explaining daily variability in larval concentrations.

Shear stress exerted by the wind alters the velocity profiles considerably. Current directions are offshore near the surface and onshore near the bottom (i.e., streaming) in the no-wind conditions, which is consistent with the model by Lentz et al. (2008). Larvae present near the bottom may be carried toward shore by streaming. The same flow pattern should be observed under offshore wind event. With onshore wind forcing, current directions become

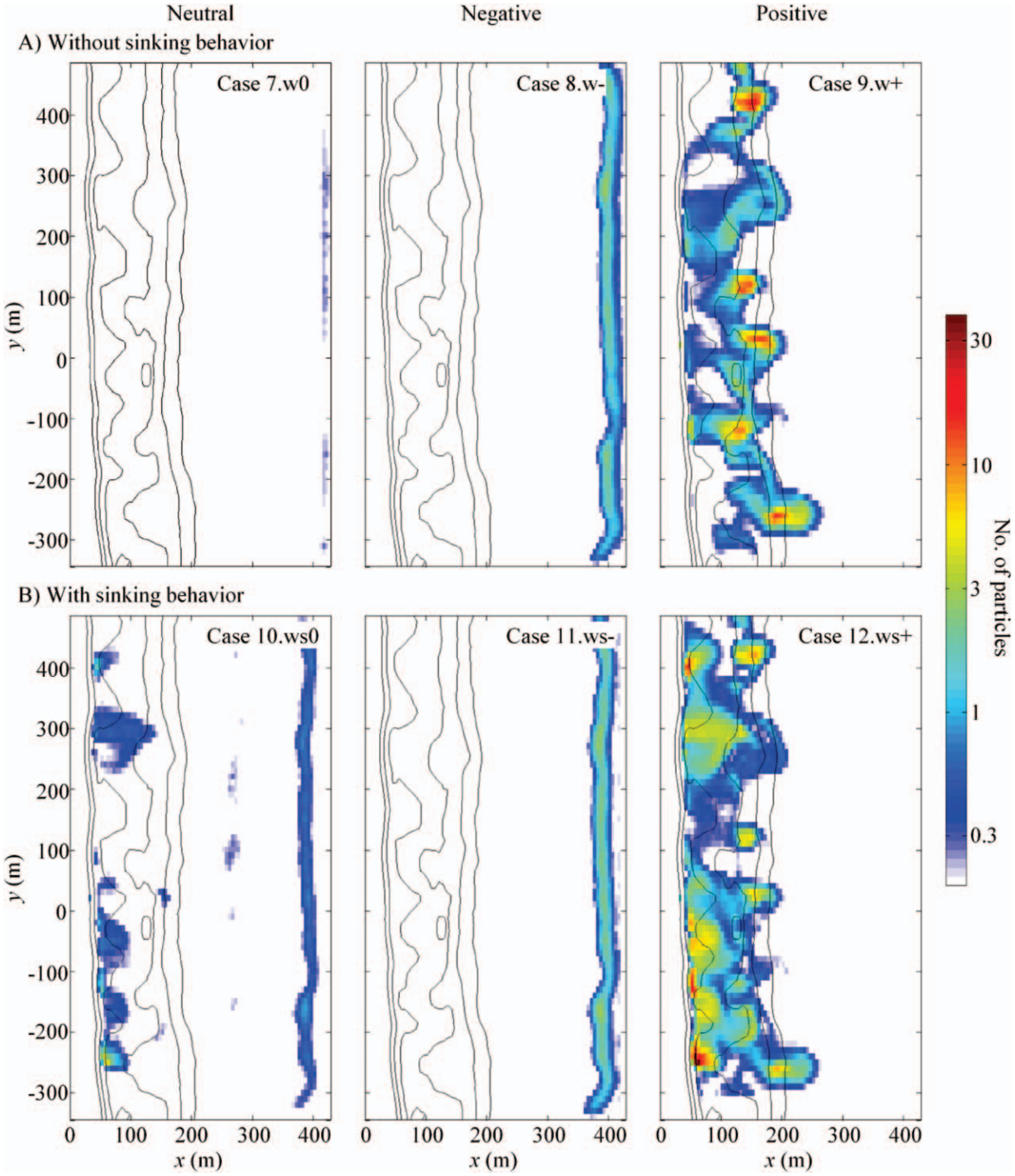

Fig. 5. Depth- and time-averaged number of particles per grid cell. Regular wave, wind, Stokes drift, with buoyancy of neutral (Cases 7.w0 and 10.ws0), negative (Cases 8.w− and 11.ws−), and positive (Cases 9.w+ and 12.ws+). (A) Particles without sinking behavior, and (B) particles with sinking behavior. Bottom contour lines from 0 m depth (shore line) to 5 m depth with 1 m increments are given. The color bar is in a log scale.

onshore near the surface and offshore near the bottom in the offshore area, and similar patterns were observed by Fewings et al. (2008). Thus, the surface flow generated by wind stress may help surface-dwelling larvae move onshore; however, the model suggests that it inhibits the onshore movement of larvae residing near the bottom.

When larvae keep floating without sinking behavior in the wind case, they tend to stack around the surf zone edge (x = 125 m) where the surface current is the result of a delicate balance between the offshore-directed mass-flux and the onshore forcing by the wind (Fig. 6). The mass flux builds up to the outer edge of the surf zone, and is

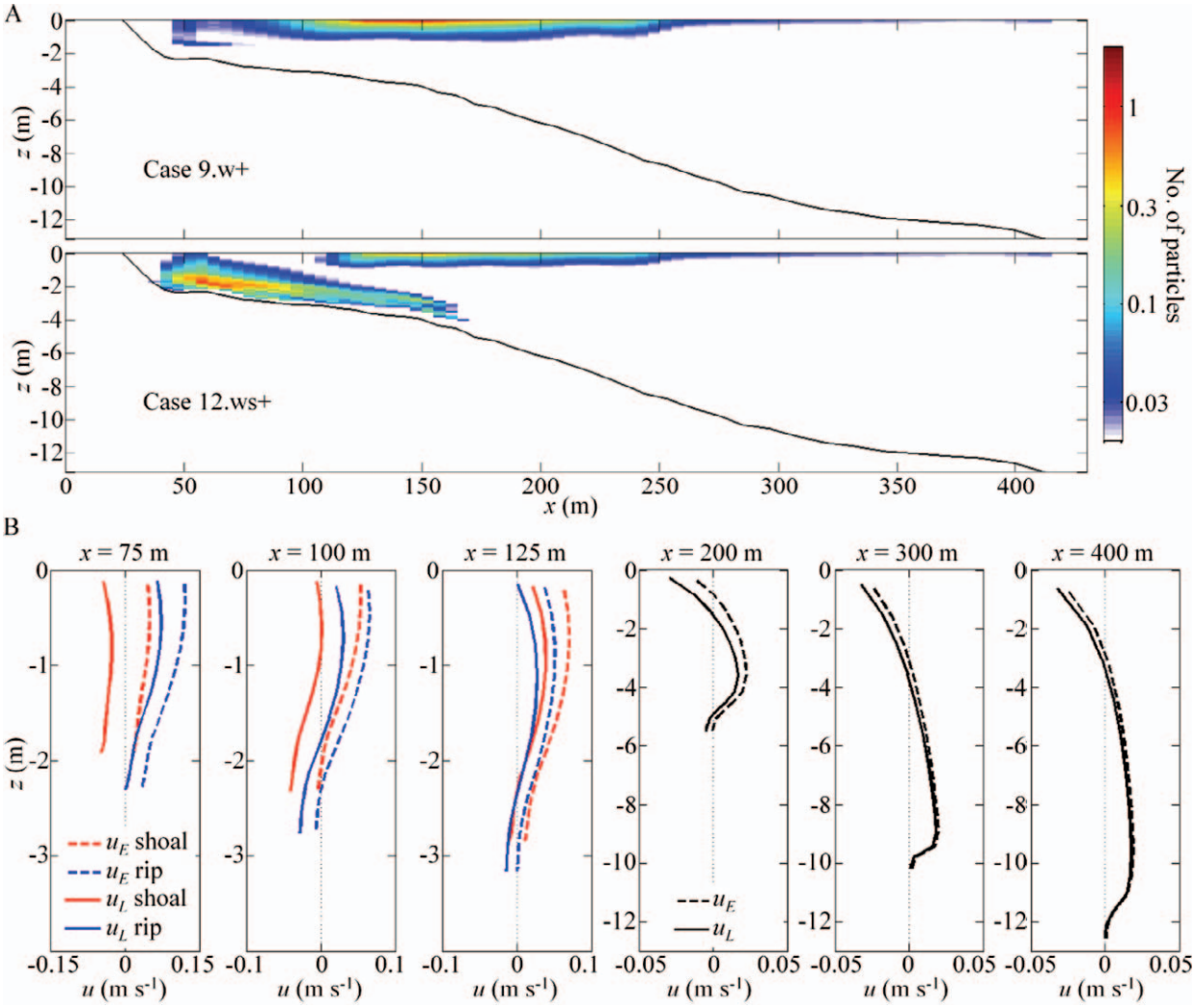

Fig. 6. (A) Alongshore- and time-averaged number of particles per grid cell. Regular wave, wind, Stokes drift, positive buoyancy, without sinking behavior (Case 9.w+) and with sinking behavior (Case 12.ws+). The maximum depth line is shown as a bottom frame. The color bar is in a log scale. (B) Vertical profiles of alongshore- and time-averaged cross-shore velocities in the physical model case of regular waves with wind. Dashed line is Eulerian velocity (u_E) and solid line is Lagrangian velocity (u_L). The first three panels to the left are average velocities in the rip channels (blue) and on the shoals (red), and the others are averages over the total alongshore ranges (black). Positive values correspond to offshore currents.

compensated over a decreasing depth, resulting in an increasing offshore velocity toward the surf zone edge. In addition, because of the intermittent breaking at the surf zone edge, the turbulent eddy viscosity at the surface is enhanced compared with further offshore, resulting in a weaker vertical shear. These two effects combined result in an offshore-directed flow at the surf zone edge. This transition from onshore- to offshore-directed surface currents in the presence of wind is not site-specific, but does depend on the wave and wind conditions.

Given the model results that larvae entering the surf zone need turbulence-dependent sinking behavior, Stokes drift, and combinations of vertical positions (i.e., larval buoyancy) and wind-dependent cross-shore flow, there are two possible scenarios that may generate cross-shore larval migration. In one scenario, negatively buoyant (or downward swimming) larvae migrate onshore without wind stress (Fig. 8A). Larvae sink and are kept in the turbulent bottom boundary layer, where turbulence is high enough to induce the sinking behavior. In the boundary layer, larvae are carried by streaming into the surf zone. In the other model scenario, positively buoyant (or upward-swimming) larvae migrate from offshore under wind forcing (Fig. 8B). Larvae drift at or near the water surface until they reach the edge of the surf zone where turbulence is high enough to induce larvae to sink, thereby avoiding offshore flow near the surface and enhancing onshore transport near the bottom. In our model with wind (Case 12.ws+), some buoyant particles are entrained by eddies in the rip-head zone around $x = 150$ m, and stay at the surface (Fig. 8B). Floating particles trapped by this type of eddies are also shown by Reniers et al. (2010).

Particles near the bottom generally are transported over the shoals first, and then typically converge in the rip

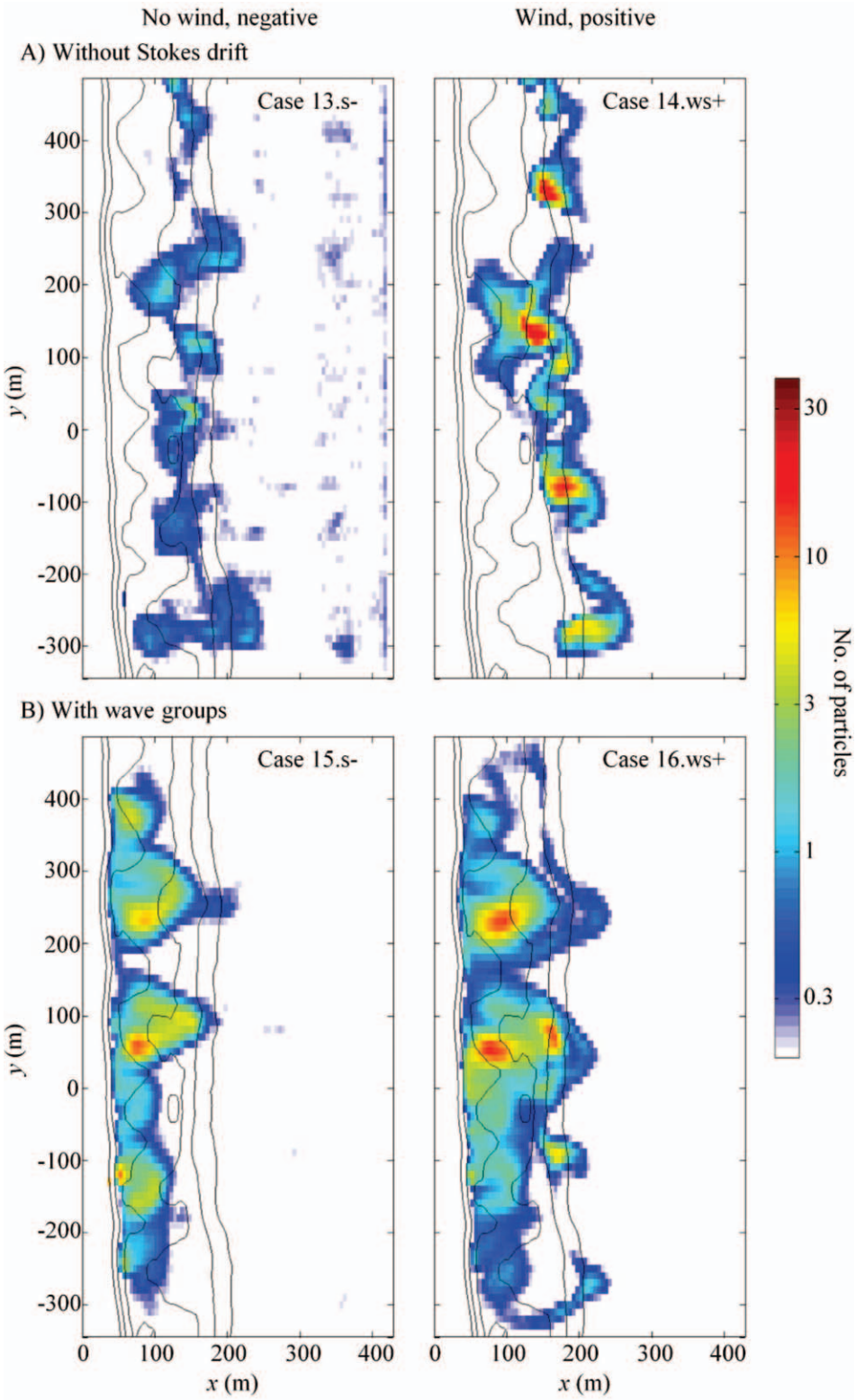

Fig. 7. (A) Depth- and time-averaged number of particles per grid cell in cases with sinking behavior, (A) regular wave, without Stokes drift, and (B) wave groups, with Stokes drift. No wind, negative buoyancy (Case 13.s−, Case 15.s−). Wind, positive buoyancy (Case 14.ws+, Case 16.ws+). These cases correspond to Cases 5.s− and 12.ws+, respectively. Bottom contour lines from 0 m depth (shore line) to 5 m depth with 1 m increments are given. The color bar is in a log scale.

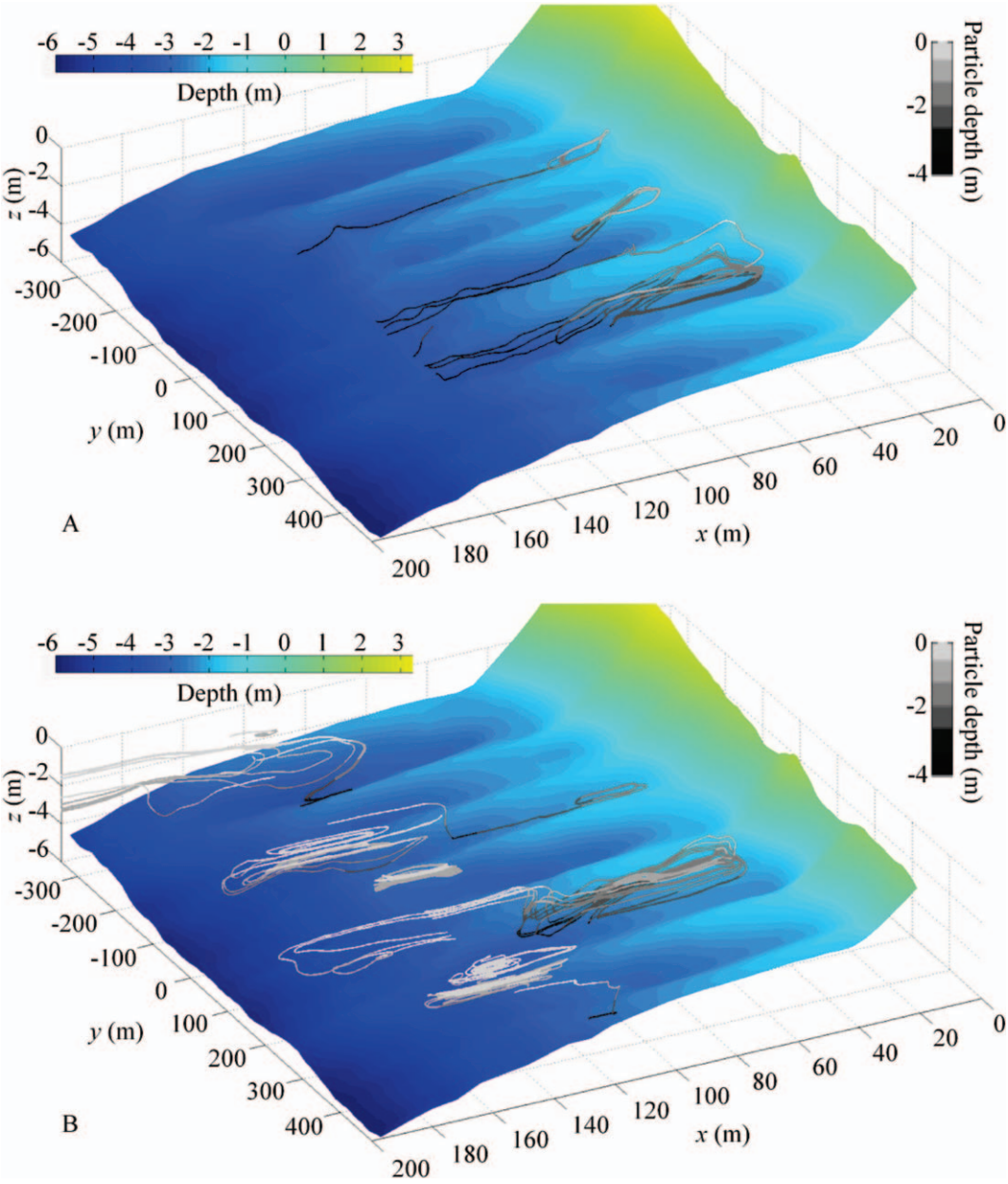

Fig. 8. Example of particle pathways in (A) Case 5s− and (B) Case 12.ws+.

channels by locally circulating (Fig. 8). After the particles enter the rip, they are carried toward the surface by upward flow and transported away from shore by return flow (Fig. 8). Once the return flow forcing becomes small, they sink again and are carried shoreward again by the bed flow, resulting in persistent circulation patterns (Fig. 8). This mechanism is unique to a rip-channeled beach with predominantly normally incident waves.

In the successful migration scenarios, the concentrations of modeled particles in rip channels are higher than on shoals and offshore (Fig. 9A). This is consistent with larval concentrations documented in the field (Fig. 9B; $p < 0.05$). Whether physical factors, such as tides and changing wave conditions, affect these concentrations is not considered here. Because our results are based on vertical velocities of competent gastropod larvae (Fuchs et al. 2004), specific density, vertical velocities, and swimming behaviors of other species probably also need to be examined to provide a species-specific model for onshore transport of larvae across the surf zone. Nevertheless, there seems to be common factor(s), such as sinking behavior, affecting patch distributions of zooplankton across taxa because statistical analysis shows that concentrations of all three taxa, including copepods as holoplankton, in the rip were significantly higher than on the shoal and offshore ($p < 0.05$), and there is no significant difference between concentrations on the shoal and offshore ($p > 0.05$; Fig. 9B). Quantified data from the successful migration model cases support the observed higher concentration of competent larvae in the surf zone compared with offshore (Table 2).

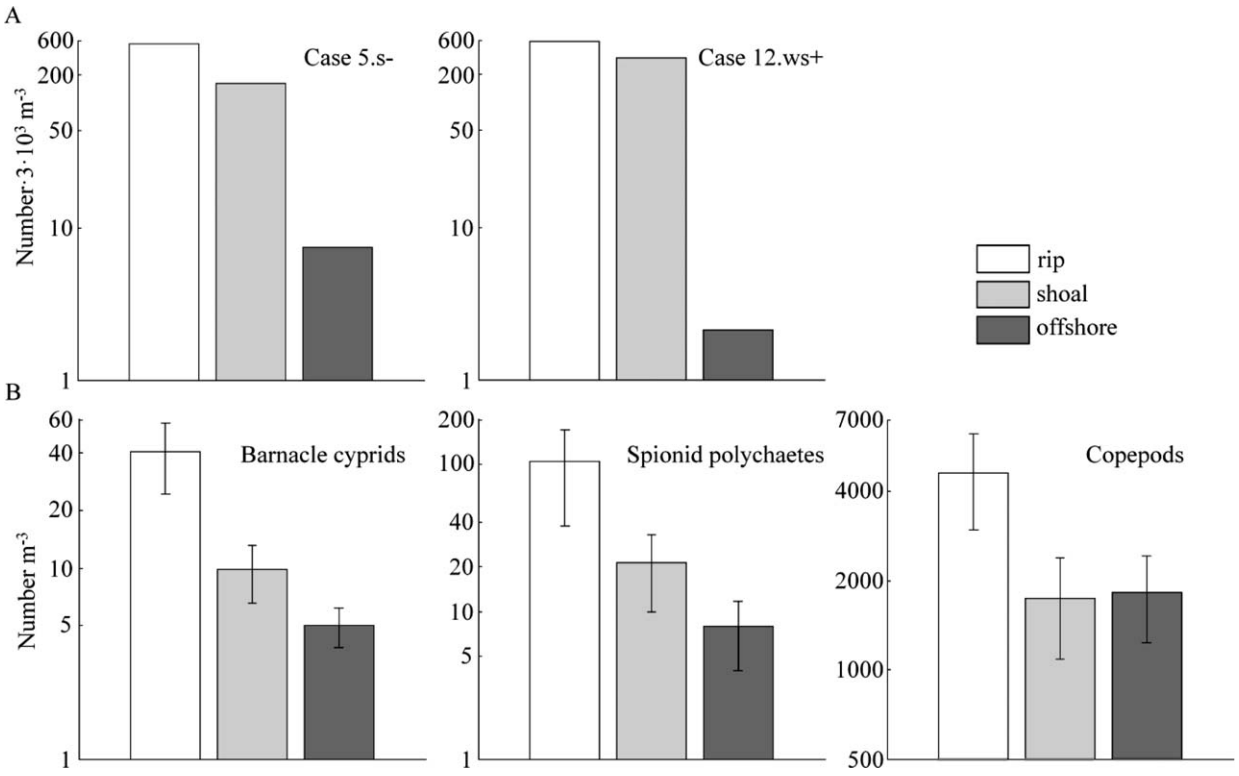

Fig. 9. (A) Time-averaged number of particles per m^3 in the rip channels ($x < 100$ m), on the shoals ($x < 100$ m), and offshore ($x > 200$ m), in cases with regular wave, sinking behavior, Stokes drift. No wind, negative buoyancy (Case 5.s−). Wind, positive buoyancy (Case 12.ws+). (B) Average concentrations (± 95% CI) of barnacle cyprids, spionid polychaetes, and copepods in the rip channel, on the shoal, and offshore in the field.

The locations and sizes of larval patches in the wave-group cases (Fig. 7B) differ from those in the regular-wave cases (Cases 5.s− and 12.ws+ in Figs. 3B and 5B, respectively). The patches in the wave-group cases are larger and concentrated at fewer locations. Although the distribution patterns differ, all of these cases achieved onshore larval transport, and resulted in higher larval concentrations in the rip channels than on the shoals, as was observed in our field results (Fig. 9).

That floating particles exit from the surf zone through rip currents is more clearly seen in Case 16.ws+ than in Case 12.ws+. This is likely a result of the generation of surf zone eddies by the incident wave groups that can temporarily trap particles. Once these eddies detach from the rip circulation, they can eject the particles offshore, forming narrow surface streaks outside of the surf zone (Reniers et al. 2010), as shown in Fig. 7B.

For longer time scales, tidal forcing also may affect larval transport (Shanks 1986; Pineda 1999); at least, timing of onshore migration could be determined by the tides. Along with the tidal cycle, diurnal wind stresses are important for long-term cross-shore transport of water, as found by Hendrickson and MacMahan (2009). Larvae residing near the bottom are transported shoreward during wind relaxation or offshore wind events, whereas larvae residing near the surface are transported shoreward during onshore wind events. Fewings et al. (2008) showed that alongshore winds do not substantially contribute to cross-shore exchange near shore and, in addition, alongshore winds were weak during the sampling period.

Although our model is simplified, it provided two reasonable scenarios of larval transport across the surf zone at a rip-channeled beach. Of course, the mechanisms we applied in this study are not exhaustive and the model can be developed with additional environmental conditions. In particular, the transport within the breaking wave roller might be of importance as mentioned earlier. The model results are representative for rip-channeled beaches only. And although this is a specific beach type, it is very common in nature. The modeled wave and flow patterns

Table 2. Ratios of particles in the rip-to-offshore and ratios of the particles on the shoal-to-offshore. The ratios in the model cases were calculated for depth-averaged and depth-integrated particles.

Model case or taxon	Rip : offshore	Shoal : offshore
5.s− (depth-averaged)	67.7	19.8
5.s− (depth-integrated)	17.8	3.1
12.ws+ (depth-averaged)	153.1	88.2
12.ws+ (depth-integrated)	40.3	13.9
Barnacle cyprid	11.8	2.3
Spionid polychaete	25.8	2.7
Copepod	3.2	1.6

within the surf zone were consistent with literature on rip-channeled beaches (Wright and Short 1984; Dalrymple et al. 2011), and outside of the surf zone the modeled flow patterns were also consistent with other studies (Fewings et al. 2008; Lentz et al. 2008). However, the surf zone circulation is affected by the bathymetry and it is worth testing with other types of beaches.

Acknowledgments

We appreciate our colleagues, technicians, and students who helped with the field experiments. We thank two anonymous reviewers and the Associate Editor James Leichter as well as Josefina Olascoaga for their valuable comments on this manuscript.

This study is supported by National Science Foundation (NSF) Ocean Sciences (OCE-092735) 'Collaborative Research: Does coupling between the inner shelf and surf zone regulate larval supply to intertidal populations?' C. Paris is funded by NSF (OCE-1155698). This is a contribution of the Rosenstiel School of Marine and Atmospheric Science, the Oregon Institute of Marine Biology, the Naval Postgraduate School, and the Bodega Marine Laboratory.

References

Connolly, S. R., B. A. Menge, and J. Roughgarden. 2001. A latitudinal gradient in recruitment of intertidal invertebrates in the northeast Pacific Ocean. Ecology **82:** 1799–1813, doi:10.1890/0012-9658(2001)082[1799:ALGIRO]2.0.CO;2

Dalrymple, R. A., J. H. MacMahan, A. J. H. M. Reniers, and V. Nelko. 2011. Rip currents. Ann. Rev. Fluid Mech. **43:** 551–581, doi:10.1146/annurev-fluid-122109-160733

Deltares. 2013*a*. Delft3D-FLOW userm, version 3.15. Delft, The Netherlands: Deltares. [accessed 08 March 2013]. Available from http://oss.deltares.nl/documents/183920/185723/Delft3D-FLOW_User_Manual.pdf

———. 2013*b*. Delft3D-WAVE user manual, version 3.05. Delft, The Netherlands: Deltares. [accessed 08 March 2013]. Available from http://oss.deltares.nl/documents/183920/185723/Delft3D-WAVE_User_Manual.pdf

Feddersen, F. 2007. Breaking wave induced cross-shore tracer dispersion in the surfzone: Model results and scalings. J. Geophys. Res. **112:** C09012, doi:10.1029/2006JC004006

Fewings, M., S. J. Lentz, and J. Fredericks. 2008. Observations of cross-shelf flow driven by cross-shelf winds on the inner continental shelf. J. Phys. Oceanogr. **38:** 2358–2378, doi:10.1175/2008JPO3990.1

Fuchs, H. L., E. J. Huter, E. L. Schmitt, and R. A. Guazzo. 2013. Active downward propulsion by oyster larvae in turbulence. J. Exp. Biol. **216:** 1458–1469, doi:10.1242/jeb.079855

———, L. S. Mullineaux, and A. R. Solow. 2004. Sinking behavior of gastropod larvae (Ilyanassa obsoleta) in turbulence. Limnol. Oceanogr. **49:** 1937–1948, doi:10.4319/lo.2004.49.6.1937

Hasselmann, K., and others. 1973. Measurements of wind-wave growth and swell decay during the Joint North Sea Wave Project (JONSWAP). Dtsch. Hydrogr. Z. Suppl. A **(8):** 12.

Hendrickson, J., and J. MacMahan. 2009. Diurnal sea breeze effects on inner-shelf cross-shore exchange. Cont. Shelf Res. **29:** 2195–2206, doi:10.1016/j.csr.2009.08.011

Kingsford, M. J., J. M. Leis, A. Shanks, K. C. Lindeman, S. G. Morgan, and J. Pineda. 2002. Sensory environments, larval abilities and local self-recruitment. Bull. Mar. Sci. **70:** 309–340.

Lentz, S. J., M. Fewings, P. Howd, J. Fredericks, and K. Hathaway. 2008. Observations and a model of undertow over the inner continental shelf. J. Phys. Oceanogr. **38:** 2341–2357, doi:10.1175/2008JPO3986.1

Longuet-Higgins, M. S. 1953. Mass transport in water waves. Philos. Trans. R. Soc. Lond. **A245:** 535–581, doi:10.1098/rsta.1953.0006

MacMahan, J., and others. 2010. Mean Lagrangian flow behavior on an open rip-channeled beach: A new perspective. Mar. Geol. **268:** 1–15, doi:10.1016/j.margeo.2009.09.011

———, A. J. H. M. Reniers, E. B. Thornton, and T. P. Stanton. 2004. Infragravity rip current pulsations. J. Geophys. Res. **109:** C01033, doi:10.1029/2003JC002068

Morgan, S. G., and J. L. Fisher. 2010. Larval behavior regulates nearshore retention and offshore migration in an upwelling shadow and along the open coast. Mar. Ecol. Prog. Ser. **404:** 109–126, doi:10.3354/meps08476

———, ———, and A. J. Mace. 2009*a*. Larval recruitment in a region of strong, persistent upwelling and recruitment limitation. Mar. Ecol. Prog. Ser. **394:** 79–99, doi:10.3354/meps08216

———, ———, ———, L. Akins, A. M. Slaughter, and S. M. Bollens. 2009*b*. Cross-shelf distributions and recruitment of crab postlarvae in a region of strong upwelling. Mar. Ecol. Prog. Ser. **380:** 173–185, doi:10.3354/meps07913

———, ———, S. H. Miller, S. T. McAfee, and J. L. Largier. 2009*c*. Nearshore larval retention in a region of strong upwelling and recruitment limitation. Ecology **90:** 3489–3502, doi:10.1890/08-1550.1

North, E. W., A. Gallego, and P. Petitgas. 2009. Manual of recommended practices for modelling physical–biological interactions during fish early life. ICES Coop. Res. Rep. 295. ICES.

Paris, C. B., J. Atema, J.-O. Irisson, M. Kingsford, G. Gerlach, and C. M. Guigand. 2013*a*. Reef odor: A wake up call for navigation in reef fish larvae. PLoS ONE **8:** e72808, doi:10.1371/journal.pone.0072808

———, L. Chérubin, and R. Cowen. 2007. Surfing, spinning, or diving from reef to reef: Effects on population connectivity. Mar. Ecol. Prog. Ser. **347:** 285–300, doi:10.3354/meps06985

———, J. Helgers, E. Van Sebille, and A. Srinivasan. 2013*b*. Connectivity modeling system: A probabilistic modeling tool for the multi-scale tracking of biotic and abiotic variability in the ocean. Environ. Modell. Softw. **42:** 47–54, doi:10.1016/j.envsoft.2012.12.006

Pineda, J. 1999. Circulation and larval distribution in internal tidal bore warm fronts. Limnol. Oceanogr. **44:** 1400–1414, doi:10.4319/lo.1999.44.6.1400

Queiroga, H., and J. Blanton. 2005. Interactions between behaviour and physical forcing in the control of horizontal transport of decapod Crustacean larvae. Adv. Mar. Biol. **47:** 107–214, doi:10.1016/S0065-2881(04)47002-3

Reniers, A. J. H. M., E. L. Gallagher, J. H. MacMahan, J. A. Brown, A. A. van Rooijen, J. S. M. van Thiel de Vries, and B. C. van Prooijen. 2013. Observations and modeling of steep-beach grain-size variability. J. Geophys. Res. **118:** 577–591, doi:10.1029/2012JC008073

———, J. H. MacMahan, F. J. Beron-Vera, and M. J. Olascoaga. 2010. Rip-current pulses tied to Lagrangian coherent structures. Geophys. Res. Lett. **37:** L05605, doi:10.1029/2009GL041443

———, and others. 2009. Surf zone retention on a rip-channeled beach. J. Geophys. Res. **114:** C10010, doi:10.1029/2008JC005153

Rilov, G., S. E. Dudas, B. A. Menge, B. A. Grantham, J. Lubchenco, and D. R. Schiel. 2008. The surf zone: A semi-permeable barrier to onshore recruitment of invertebrate larvae? J. Exp. Mar. Biol. Ecol. **361:** 59–74, doi:10.1016/j.jembe.2008.04.008

Roy, A., A. Metaxas, and T. Ross. 2012. Swimming patterns of larval Strongylocentrotus droebachiensis in turbulence in the laboratory. Mar. Ecol. Prog. Ser. **453:** 117–127, doi:10.3354/meps09662

Shanks, A. L. 1986. Tidal periodicity in the daily settlement of intertidal barnacle larvae and an hypothesized mechanism for the cross-shelf transport of cyprids. Biol. Bull. **170:** 429–440, doi:10.2307/1541852

———. 1995. Oriented swimming by megalopae of several eastern North Pacific crab species and its potential role in their onshore migration. J. Exp. Mar. Biol. Ecol. **186:** 1–16, doi:10.1016/0022-0981(94)00144-3

———, S. G. Morgan, J. MacMahan, and A. J. H. M. Reniers. 2010. Surfzone hydrodynamics as determinants of temporal and spatial variation in larval recruitment. J. Exp. Mar. Biol. Ecol. **392:** 140–150, doi:10.1016/j.jembe.2010.04.018

———, and R. K. Shearman. 2009. Paradigm lost? Cross-shelf distributions of intertidal invertebrate larvae are unaffected by upwelling or downwelling. Mar. Ecol. Prog. Ser. **385:** 189–204, doi:10.3354/meps08043

Staaterman, E., C. B. Paris, and J. Helgers. 2012. Orientation behavior in fish larvae: A missing piece to Hjort's critical period hypothesis. J. Theor. Biol. **304:** 188–196, doi:10.1016/j.jtbi.2012.03.016

Stokes, G. G. 1847. On the theory of oscillatory waves. Trans. Cambridge Philos. Soc. **8:** 441–455.

Vermeij, M. J. A., K. L. Marhaver, C. M. Huijbers, I. Nagelkerken, and S. D. Simpson. 2010. Coral larvae move toward reef sounds. PLoS ONE **5:** e10660, doi:10.1371/journal.pone.0010660

Wright, L. D., and A. D. Short. 1984. Morphodynamic variability of surf zones and beaches. Mar. Geol. **56:** 93–118, doi:10.1016/0025-3227(84)90008-2

Associate editor: James J. Leichter

Received: 11 October 2013
Accepted: 05 March 2014
Amended: 03 May 2014